JACS
JOURNAL OF THE AMERICAN CHEMICAL SOCIETY
Article
pubs.acs.org/JACS

Large Entropic Effects on the Thermochemistry of Silicon Nanodusty Plasma Constituents

Prasenjit Seal and Donald G. Truhlar*

Department of Chemistry, Supercomputing Institute, and Chemical Theory Center, University of Minnesota, Minneapolis, Minnesota 55455-0431, United States

Supporting Information

ABSTRACT: Determination of the thermodynamic properties of reactor constituents is the first step in designing control strategies for plasma-mediated deposition processes and is also a key fundamental issue in physical chemistry. In this work, a recently proposed multistructural statistical thermodynamic method is used to show the importance of multiple structures and torsional anharmonicity in determining the thermodynamic properties of silicon hydride clusters, which are important both in plasmas and in thermally driven systems. It includes five different categories of silicon hydride clusters and radicals, including silanes, silyl radicals, and silenes. We employed a statistical mechanical approach, namely the recently developed multistructural (MS) anharmonicity method, in combination with density functional theory to calculate the partition functions, which in turn are used to estimate thermodynamic quantities, namely Gibbs free energy, enthalpy, entropy, and heat capacity, for all of the systems considered. The calculations are performed using all of the conformational structures of each molecule or radical by employing the multistructural quasiharmonic approximation (MS-QH) and also by including torsional potential anharmonicity (MS-T). For those cases where group additivity (GA) results are available, the thermodynamic quantities obtained from our MS-T calculations differ considerably due to the fact that the GA method is based on single-structure data for isomers of each stoichiometry, and hence lack multistructural effects; whereas we find that multistructural effects are very important in silicon hydride systems. Our results also indicate that the entropic effect on the thermochemistry is huge and is dominated by multistructural effects. The entropic effect of multiple structures is also expected to be important for other kinds of chain molecules, and its effect on nucleation kinetics is expected to be large.

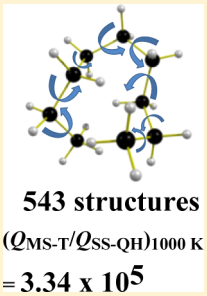

INTRODUCTION

Plasmas containing dispersed particulates, so-called "dusty plasmas", are ubiquitous in the universe, are important in industry,[1,2] and involve many phenomena not found in either neutral aerosols or in plasmas that do not contain particulates.[3,4] Plasmas that contain very small particles (less than 100 nm in diameter) are of particular interest because particulates of this size are a major source of contamination of wafers in semiconductor processing. These contaminants include nanoparticles generated by gas-phase nucleation in the chemically reacting plasmas used for thin film deposition and etching. As microelectronics feature sizes have shifted deeper into the nanoscale regime, the need to avoid contaminant nanoparticles has become more critical, and understanding the mechanisms for such particle formation (nucleation) and growth is essential. The nucleation is governed by chemical reactions and interplay between growth and charging of molecular clusters and by transport of these clusters by electric forces and diffusion.

Silane plasmas are of special interest because they are widely used to grow microcrystalline silicon for electronics and amorphous hydrogenated silicon for photovoltaics, as well as, more recently, silicon nanocrystals that show promise for photovoltaics and photonics. Mass spectrometry studies demonstrated that silicon hydride neutral and cation clusters are limited to smaller sizes.[3] Silanes are the most studied chemical species in nanodusty plasmas,[1−20] but a realistic mechanism[4,21−23] also includes radicals and unsaturated species, which are included in the present study, and ions, which are not.

The mechanistic analysis of silane plasmas starts with thermodynamic data.[24] Katzer et al.[2] reported enthalpies, entropies, and Gibbs formation energies for several categories of silicon hydrides (silanes, silyl radicals, silylenes, etc.) with 1−5 silicon atoms. Later, Swihart and Girshick[3] studied the reaction mechanisms for silicon hydride cluster formation during silane pyrolysis. They estimated and reported the thermochemistry parameters of silicon hydrides using group additivity methods. Bhandarkar and co-workers[4] developed a silicon hydride clustering model in order to study the nucleation of particles in low-temperature silane plasmas; their model includes silyl radicals and anions. Li et al.[5] have reported the molecular structures, electron affinities, and dissociation energies for Si_5H_n and $Si_5H_n^-$ clusters by means of density functional theory, while in an earlier work, Xu et al.[6] have studied the same for the Si_3 clusters. Swihart[7] reported the adiabatic electron affinities of 72 hydrogenated silicon clusters up to seven silicon atoms; the electron affinities were found to increase with an increase in cluster size. Wong et al.[8] reported

Received: October 16, 2013
Published: January 16, 2014

dx.doi.org/10.1021/ja410498d | J. Am. Chem. Soc. 2014, 136, 2786−2799

the thermochemical properties of silicon hydrides using various theoretical methods. They also performed a detailed kinetic modeling of silicon nanoparticle formation chemistry. Recently, Oyedepo et al.[10] used multireference correlation consistent composite calculations of atomization energies, and enthalpies of formation for silicon hydrides, aluminides, and phosphorides to study the ground and lowest-lying spin-forbidden excited states for a series of Si-containing systems.

Previous investigations also include larger silicon clusters. Chang et al.[11] reported the geometries, energetics, and electronic properties for charged phosphorus-doped silicon clusters, PSi_n^+ and PSi_n^-. Yang et al.[12] investigated the molecular structures, electron affinities, and dissociation energies for Si_nH and Si_nH^- clusters up to 10 Si atoms. Adamczyk and Broadbelt[13] studied the thermochemical properties of Si clusters of size 13 using statistical thermodynamics for a temperature range of 298−6000 K. Ågren and co-workers[14] calculated the linear polarizabilities and second order hyperpolarizabilities for one-, two-, and three-dimensional hydrogen-terminated Si clusters in the random phase approximation.

Although there are numerous investigations of the hydrogenated Si clusters, there are no explorations of the role of multiple conformational structures, internal rotations or torsions, or the associated entropic effects present in these systems. Here we established the role of multiple structures and torsional anharmonicities in determining the partition functions and thermodynamic properties for different sizes and types of Si_nH_m clusters, and we demonstrated and quantified the effect of the increased entropies on the thermochemistry of these clusters. Not only do the calculations treat the multiple-structure problem more completely than does past work, but also they use efficient multilevel quantum mechanical methods[25] for energetic calcuations and a chemically accurate density functional[26] for efficient structure determination.

Coupled torsions have been studied in several recent papers on a variety of systems.[27−40] Of particular relevance is that the internal-coordinate multistructural (MS) approximation for torsional (T) anharmonicity[27,28] has been used to compute partition functions and other thermodynamic quantities of hydrocarbons[29,30] and other organic species.[31−35] Here we apply the method to hydrogenated silicon clusters.

THEORY AND COMPUTATIONAL DETAILS

Throughout the work, we use the word "structure" as a synonym for "conformation". At a fundamental level, multiple conformations of complex molecules are a manifestation of anharmonicity (an harmonic potential has only a single minimum and the presence of multiple local minima on a potential energy surface is therefore an anharmonic effect). In the treatment used here, the problem of multiple conformations is recast in terms of conformational entropy and anharmonicity, In particular, we have included anharmonicity in three ways:

1. Using a complete set of all structures for each species;
2. Including torsional potential anharmonicity and the coupling of torsions to one another and to overall rotation; and
3. Scaling of harmonic frequencies by empirical factors[41] that depend on the electronic model chemistry; this quasiharmonic (QH) approach is used to reduce the error in zero-point energies as compared to those calculated by the local harmonic approximation.

The multistructural torsional anharmonicity (MS-T) method for determining the partition functions and thermodynamic quantities takes into account all of the conformational structures of a given system and thereby improves over the quasi harmonic (QH) results. In the present work, we employed two methods of MS-T, i.e., the recent MS-T(C) method[28] based on the coupled torsional potential and the older MS-T(U) method,[27] which is based on uncoupled torsional potential. Results are given in the main article only for the MS-T(C) method, and only at a limited set of temperatures to show the main trends, but full sets of MS-T(C) and MS-T(U) results at a large number of temperatures are given in the Supporting Information (SI), Tables S1−S8. Next, we review the equations for the coupled potential version;[28] the reader is referred to the original publication[27] for discussion of the uncoupled potential version.

MS-T(C) Method. For a particular system, when torsions are coupled, we assume that each coupled torsion η for a structure j has a reference potential given by the following:[28]

$$V_{j,\eta} = U_j + \frac{W_{j,\eta}^{(C)}}{2}[1 - \cos M_{j,\eta}(\phi_{j,\eta} - \phi_{j,\eta,eq})]; \quad \frac{-\pi}{M_{j,\eta}} \le \phi_{j,\eta} - \phi_{j,\eta,eq} \le \frac{\pi}{M_{j,\eta}} \tag{1}$$

where U_j is the energy of structure j (the global minimum is set to 0), $W_{j,\eta}^{(C)}$ is effective coupled torsional barrier height, $M_{j,\eta}$ is a local periodicity parameter, $\phi_{j,\eta}$ is torsional coordinate, and $\phi_{j,\eta,eq}$ is the torsional coordinate at the equilibrium geometry.

For a molecule with J distinguishable structures and t torsions, the conformational-rovibrational partition function according to the MS-T(C) method is as follows:[28]

$$Q_{con\text{-}rovib}^{MS\text{-}T(C)} = \sum_{j=1}^{J} Q_{rot,j} \exp(-\beta U_j) Q_j^{QH} \prod_{\eta=1}^{t} \tilde{f}_{j,\eta} \tag{2}$$

where

$$Q_j^{QH} = \prod_{i=1}^{F} \frac{\exp(-\beta\hbar\omega_{j,i}/2)}{1 - \exp(-\beta\hbar\omega_{j,i})} \tag{3}$$

Here $Q_{rot,j}$ is the rotational partition function of structure j, β is $1/k_BT$ in formulae (above and eq 4) using molecular units and is $1/RT$ in formulas (eqs 5 and later) using molar units (where k_B is Boltzmann's constant, T is temperature, and R is the gas constant), Q_j^{QH} is the usual normal-mode quasiharmonic oscillator vibrational partition function calculated at structure j, $\tilde{f}_{j,\eta}$ is a factor that takes account of torsional potential anharmonicity, F is number of degrees of freedom for vibrational modes, and $\omega_{j,i}$ denotes the scaled normal-mode vibrational frequency of mode i of structure j. The zero of energy for Q_j^{QH} is at the local minimum of the potential energy function for structure j, not at the zero point level of structure j.

We use the classical expression for the rotational partition function for structure j,

$$Q_{rot,j} = \frac{\sqrt{\pi}}{\sigma_{rot,j}} \left(\frac{2}{\hbar^2\beta}\right)^{3/2} \sqrt{I_{A,j} I_{B,j} I_{C,j}} \tag{4}$$

where $\sigma_{rot,j}$ is the symmetry number of overall rotation, and $I_{A,j}$, $I_{B,j}$, and $I_{C,j}$ are the principal moments of inertia.

If the $\tilde{f}_{j,\eta}$ are set to unity, then the partition function $Q_{con\text{-}rovib}^{MS\text{-}T(C)}$ reduces to the multistructural quasiharmonic (MS-QH) partition function. However, when it is approximated by the MS-T(C) method, the partition function includes the transition to hindered internal rotors as the temperature is raised such that the average energy begins to exceed the torsional barriers, and it includes the transition to a free internal rotor limit as the temperature is raised even higher. The low-temperature limit is based on consistently coupled torsional frequencies. The determination of the effective coupled torsional barrier heights of eq 1 includes the torsional potential anharmonicity. The high-temperature free rotor limit includes the kinetic energy coupling of the torsions to each other and to overall rotation.[28]

Thermodynamic Quantities. The total partition function is the product of the contributions of electronic, translational, and conformational−rotational−vibrational factors. From the partition

dx.doi.org/10.1021/ja410498d | J. Am. Chem. Soc. 2014, 136, 2786−2799

functions, we can calculate the standard-state enthalpy (H_T°), entropy(S_T°), heat capacity ($C_p^\circ(T)$), and Gibbs free energy (G_T°) by the standard methods of statistical thermodynamics as coded in the *MSTor* program. In particular, the thermodynamic properties are estimated at a standard pressure of 1 bar by using the following expressions.

$$G_T^\circ = -RT \ln(Q) + RT \tag{5}$$

$$H_T^\circ = -\frac{\partial \ln Q}{\partial \beta} + RT \tag{6}$$

$$S_T^\circ = R \ln Q - \frac{1}{T}\left(\frac{\partial \ln Q}{\partial \beta}\right) \tag{7}$$

and

$$C_p^\circ(T) = \frac{H^\circ(T - 2\delta T) - 8H^\circ(T - \delta T) + 8H^\circ(T + \delta T) - H^\circ(T + 2\delta T)}{12\delta T} \tag{8}$$

where R is the gas constant, and δT is a step size for a four-point central finite difference formula; in the present study, we used $\delta T = 0.5$ K.

Geometries, Basis Sets, and Software. All of the geometry optimizations and vibrational frequency calculations are performed by the M06-L[42]/6-311+G(3d2f, 2p)[43] method with frequencies scaled[41] by 0.978. The 6-311+G(3d2f, 2p) basis is the same as MG3S[44] for H and Si, and we will use the shorter name "MG3S" throughout this work. The geometry optimizations of all distinguishable structures are performed using the *GAUSSIAN 09*[45] program. The optimized Cartesian coordinates for the global minimum structure for each of the species are provided in the SI. After the structure search, the partition functions and the thermodynamic properties are calculated taking account of all structures for each system by using the *MSTor* program[46,47] and the corresponding Hessians obtained from the formatted checkpoint files.

Heats of Formation and Choice of Electronic Structure Method. In the present work, we calculated the standard-state heats of formation for Si_nH_m at 298 K, $\Delta H_{f,298}^\circ(Si_nH_m)$, and Tables 1 and 2 compare them with the group additivity values and with the empirically corrected wave function calculations of Wong et al.,[8] Ho et al.,[9] and Katzer et al.,[2] and also with the experiment.[48−50] Note that the empirical results of Wong et al. are those upon which the bond additivity parameters are based, and in that case, the empirical correction takes the form of a bond additivity correction (BAC).

For our own results, the heats of formation of Si_nH_m at 298 K are calculated from the atomization energy using the following equations.

$$\Delta H_{f,298}^\circ(Si_nH_m) = [n\Delta H_{f,298}^\circ(Si) + m\Delta H_{f,298}^\circ(H)] - \Delta H_{a,298}^\circ(Si_nH_m) \tag{9}$$

The heats of formation of atomic silicon and atomic hydrogen are taken from the JANAF tables.[51] The values are $\Delta H_{f,298}^\circ(Si) = 107.55$ kcal/mol and $\Delta H_{f,298}^\circ(H) = 52.10$ kcal/mol, respectively. In eq 9, $\Delta H_{a,298}^\circ(Si_nH_m)$ is the atomization energy, which is defined as the change in enthalpy upon decomposition of a molecule to its constituent atoms. It can be evaluated as follows:

$$\Delta H_{a,298}^\circ(Si_nH_m) = [nH_{298}^\circ(Si) + mH_{298}^\circ(H)] - H_{298}^\circ(Si_nH_m) \tag{10}$$

All of the quantities in the equations above are obtained from quantum mechanical electronic structure calculations. In order to decide which electronic structure method to use, we considered several methods that are affordable even for larger systems, and we tested them for the smaller molecules, where we tested a variety of methods for the smaller molecules where some accurate data are available. The methods studied include the use of the M06-L density functionals, four doubly hybrid density functional methods (MC3MPWB95,[52] MC3BB,[53] MCQCISD-TS,[52] and MCG3-MPW[52]), and six multilevel wave function methods based on scaling (SAC/3,[54] MCQCISD/3,[54] BMC-CCSD,[55] MCQCISD-TS,[52] G3SX(MP3),[56] and G3SX[56]). These tests are shown in Table 1. The table shows that BMC-CCSD//M06-L/MG3S gives a smaller error with respect to the experimental result than the other methods tested for silanes. However, for silenes, G3SX(MP3)//M06-L/MG3S provides the best results. Hence, we chose these two methods to compute $\Delta H_{f,298}^\circ(Si_nH_m)$. We also calculated the $\Delta H_{f,298}^\circ(Si_nH_m)$ values for one silyl radical, Si_2H_5 whose experimental value is available. The G3SX(MP3) method gives the best results for that radical and agrees with the experiment[50] within 0.07 kcal/mol. The heats of formation at 298 K for all of the silanes and silenes studied here and for Si_2H_5 radical are given in Table 2. The table shows that our values agree with the group additivity values of Wong et al.[8] only to within 2.4 kcal/mol, whereas they agree with the BAC data of Wong et al. within 1.0 kcal/mol and with the experimental data[49,50,57] within 0.3 kcal/mol. Compared to the empirical results of work of Ho et al.,[9] our multistructural results agree to within 2.7 kcal/mol.

Table 1. Method Validation[a]

methods	$\Delta H_{f,298}^\circ$ (kcal/mol)		
	Si_2H_4	Si_2H_6	Si_2H_5
group additivity model of Wong et al.[b]	67.1	21.5	
M06-L/MG3S// M06-L/MG3S	49.3	−5.1	33.3
SAC/3//M06-L/MG3S	82.3	34.7	69.2
MC3MPWB95// M06-L/MG3S	72.0	24.5	59.3
MC3BB//M06-L/MG3S	70.5	22.6	57.7
MCQCISD/3// M06-L/MG3S	67.2	19.7	56.8
BMC-CCSD// M06-L/MG3S	67.3	19.1	56.2
MCQCISD-TS// M06-L/MG3S	65.3	17.2	53.5
MCG3/3// M06-L/MG3S	64.2	4.4	43.8
MCG3-MPW// M06-L/MG3S	62.0	13.4	50.7
G3SX(MP3)// M06-L/MG3S	65.8	18.7	56.0
G3SX//M06-L/MG3S	65.6	17.9	55.3
expt.	65.73 ± 0.96[c]	19.05 ± 0.31[d]	55.93 ± 1.20[e]
Ho et al.[f] (empirical)	57.1 ± 10.0	19.1 ± 0.3	55.7 ± 3.0
Wong et al.[g] (empirical)	65.9	19.3	
Katzer et al.[h] (empirical)	67.2	19.1	56.03

[a]The methods (except for the last four rows, which are experimental or empirical) are listed in order of increasing cost (MC3MPWB95 and MC3BB have the same cost). [b]Ref 8; GA. [c]Ref 48. [d]Ref 49. [e]Ref 50. [f]Ref 9. [g]Ref 8; G3//B3LYP+BAC. [h]Ref 2.

In the work, the BMC-CCSD//M06-L/MG3S data for the thermodynamic properties are tabulated at 298 and 1000 K for all the silanes and G3SX(MP3)//M06-L/MG3S data are given for the silyl radicals and silenes. (As usual, A//B denotes using method A for single-point energy calculations at geometries optimized by method B.) The figures are plotted using BMC-CCSD//M06-L/MG3S values for the silanes and G3SX(MP3)//M06-L/MG3S values are taken for the plotting of silyl radicals and silenes. In the SI, we provide results for M06-L/MG3S, BMC-CCSD//M06-L/MG3S, and G3SX(MP3)//M06-L/MG3S at a large number of temperatures ranging from 298 to 1500 K.

Enthalpy of Atomization and Energy of Atomization. The enthalpy of atomization, ΔH_0^{298} at 298 K and the energy of atomization, ΔE, which is the change in electronic energy and nuclear repulsion that is the change in potential energy for nuclear motion, for

dx.doi.org/10.1021/ja410498d | J. Am. Chem. Soc. 2014, 136, 2786−2799

Table 2. Heats of Formation at 298 K from the Present Work Compared to the Group Additivity Parameters of Wong et al. (Ref 8), to Experiment, and to Empirical Results

	$\Delta H^{\circ}_{f,298}$ (kcal/mol)				
molecule	present work[a]	GA[b]	expt.	emp.	BAC[c]
Single-Structure Silanes (BMC-CCSD//M06-L/MG3S)					
Si_2H_6	19.1	21.5	19.1 ± 0.3[d]	19.1,[e] 19.1[f]	19.3
Si_3H_8	28.6	30.2	28.9 ± 1.0[g]	28.5,[e] 28.8[f]	28.8
Fully Branched Silanes (BMC-CCSD//M06-L/MG3S)					
Si_4H_{10}-FB	36.2	36.4		37.5[f]	36.2
Si_5H_{12}-FB	41.9	41.5		45.0[f]	41.7
Si_6H_{14}-FB	50.1	50.3			50.0
Si_7H_{16}-FB	56.4	56.4			56.4
S-Si_9H_{20}-FB	70.5	71.3			
R-Si_9H_{20}-FB	70.8				
$Si_{10}H_{22}$-FB	75.4	76.5			
Branched Silane (BMC-CCSD//M06-L/MG3S)					
iso-Si_7H_{16}	62.2	62.5			
Unbranched Silanes (BMC-CCSD//M06-L/MG3S)					
Si_4H_{10}	37.8	38.9		38.3[f]	37.9
Si_5H_{12}	46.4	47.6		47.7[f]	46.8
Si_6H_{14}	55.4	56.3			
Si_7H_{16}	64.6	65.1			
Si_8H_{18}	73.1	73.8			
Si_9H_{20}	81.6	82.5			
Single-Structure Silene (G3SX(MP3)//M06-L/MG3S)					
Si_3H_6	71.7	72.6		74.6[f]	72.1
Fully Branched Silenes (G3SX(MP3)//M06-L/MG3S)					
Si_4H_8-FB	75.9	76.7		81.0[f]	
Si_5H_{10}-FB	81.3	82.3		87.9[f]	
Si_6H_{12}-FB	90.3	92.7			93.0
Single-Structure Silyl Radical (G3SX(MP3)//M06-L/MG3S)					
Si_2H_5	56.0		55.9 ± 1.2[h]	55.7,[e] 56.0[f]	

[a]The method used in the present work is given in parentheses on the section heading; the notation used is that A//M06-L/MG3S denotes single-point energies by method A, with M06-L/MG3S used for geometries and frequencies. [b]Heats obtained from the group additivity parameters of Wong et al. [c]Bond additivity corrected G3//B3LYP values from ref 8. [d]Ref 49. [e]Empirically corrected wave function calcuations from ref 9. [f]Empirically corrected wave function calculations from ref 2. [g]Ref 57. [h]Ref 50.

each species are calculated and given in Table 3. These quantities are determined using reactions with the following stoichiometry:

$$Si_nH_m \rightarrow nSi(^3P) + mH(^2S)$$

The enthalpies of atomization are smaller in magnitude than the potential energies of atomization, and with increase in chain length, the difference in these two values becomes larger. In the case of unbranched silanes, the difference increases from 53.0 to 109.3 kcal/mol.

RESULTS AND DISCUSSION

A key issue for the structures considered in this work is the extent of branching. For structures with two or three Si atoms, no branching is possible, and for this size range we consider silanes, silyl radicals, and one silene. We also consider structures with four to ten Si atoms for which branching is possible. The additional structures are generated by torsions that are internal rotations around Si−Si bonds. We will consider unbranched and fully branched silanes and silyl radicals, one branched silane, and fully branched silenes. The unbranched silanes are

Table 3. Enthalpy of Atomization at 298 K, ΔH°_{298}, and Potential Energy[a] of Atomization, ΔE, for All Species

species	ΔH°_{298} (kcal/mol)	ΔE (kcal/mol)
Silanes (Single-Structure)[b]		
Si_2H_6	499.9	530.9
Si_3H_8	699.1	741.0
Fully Branched Silanes (Single-Structure)[b]		
Si_4H_{10}-FB	900.3	953.3
Si_5H_{12}-FB	1103.6	1167.5
Si_6H_{14}-FB	1304.0	1379.0
Si_7H_{16}-FB	1506.3	1592.5
Si_9H_{20}-FB (*S*-conformer)	1909.7	2017.7
Si_9H_{20}-FB (*R*-conformer)	1909.3	2017.6
$Si_{10}H_{22}$-FB	2113.4	2233.1
Branched Silane[b]		
iso-Si_7H_{16}	1501.2	1587.4
Unbranched Silanes[b]		
Si_4H_{10}	898.6	951.6
Si_5H_{12}	1098.9	1162.9
Si_6H_{14}	1299.3	1374.2
Si_7H_{16}	1499.5	1585.6
Si_8H_{18}	1700.1	1797.7
Si_9H_{20}	1900.4	2009.7
Branched Silyl Radicals (Single-Structure)[c]		
Si_2H_5	412.4	437.5
Si_3H_7	614.8	651.3
Si_4H_9-FB	818.9	866.6
Si_5H_{11}-FB	1019.2	1077.2
Si_6H_{13}-FB	1222.7	1292.2
Si_7H_{15}-FB	1427.2	1508.3
Unbranched Silyl Radicals[c]		
Si_4H_9, type I	813.4	860.5
Si_4H_9, type II	815.8	863.2
Si_5H_{11}, type I	1014.4	1072.6
Si_5H_{11}, type II	1016.7	1075.2
Si_5H_{11}, type III	1017.1	1075.6
Si_6H_{13}, type I	1215.6	1284.9
Si_6H_{13}, type II	1218.3	1288.2
Si_6H_{13}, type III	1218.5	1288.3
Silenes (Single-Structure)[c]		
Si_3H_6	554.5	585.8
Si_4H_8-FB	759.1	801.7
Si_5H_{10}-FB	962.3	1016.3
Si_6H_{12}-FB	1162.4	1226.6

[a]Potential energy (for nuclear motion) is the sum of electronic energy and nuclear repulsion for the lowest-energy structure (and potential energy of atomization is the increase in potential energy upon atomization). In contrast, the enthalpy of atomization is based on a multistructural calculation by the MS-T(C) method. [b]These results are calculated by BMC-CCSD//M06-L/MG3S. [c]These results are calculated by G3SX(MP3)//M06-L/MG3S.

the normal silanes (*n*-silanes). The branched silane we consider is 2-silylhexasilane, which we abbreviate as *iso*-Si_7H_{16}. Except for the fully branched silanes, the unbranched and branched species have multiple structures, i.e., multiple conformations that correspond to local minima (including the global minimum) on the potential energy surface. The fully branched species have only a single structure; we denote fully branched species in tables with the suffix "-FB". (We use this notation because we cannot use the notation "neo". Neopentasilane and neohexasilane are the same as what we call fully branched; however, for neoheptasilane and higher clusters, the prefix

dx.doi.org/10.1021/ja410498d | J. Am. Chem. Soc. 2014, 136, 2786−2799

"neo" only refers to the 2,2-disilyl groups along the chain and so the neo form of higher clusters is not fully branched in the sense of the fully branched structures of the present work. Hence, we coined the "-FB" notation.) Figure 1 illustrates the lowest-energy structures for representatives of the various classes of species considered.

Silanes. First we consider branched and unbranched silanes, Si_nH_{2n+2}. The total number of torsions present in each such molecule is $n - 1$ (see Table 4). Branching becomes possible, starting with $n = 4$. In the present investigation, we consider up to $n = 10$ for the fully branched silanes and up to $n = 9$ for *n*-silanes. For the fully branched silanes, calculations with $n = 8$ (Si_8H_{18}-FB) with the chemical formula $Si(SiH_3)_3{-}Si(SiH_3)_3$, are not included since optimization of that system under the level of theory considered (M06-L/MG3S) is not converged. This might be attributed to the strong steric hindrance exerted by the three $-SiH_3$ groups. The role of multiple structures and torsional potential anharmonicities are reflected in the partition function values for species having more than one distinguishable structure.

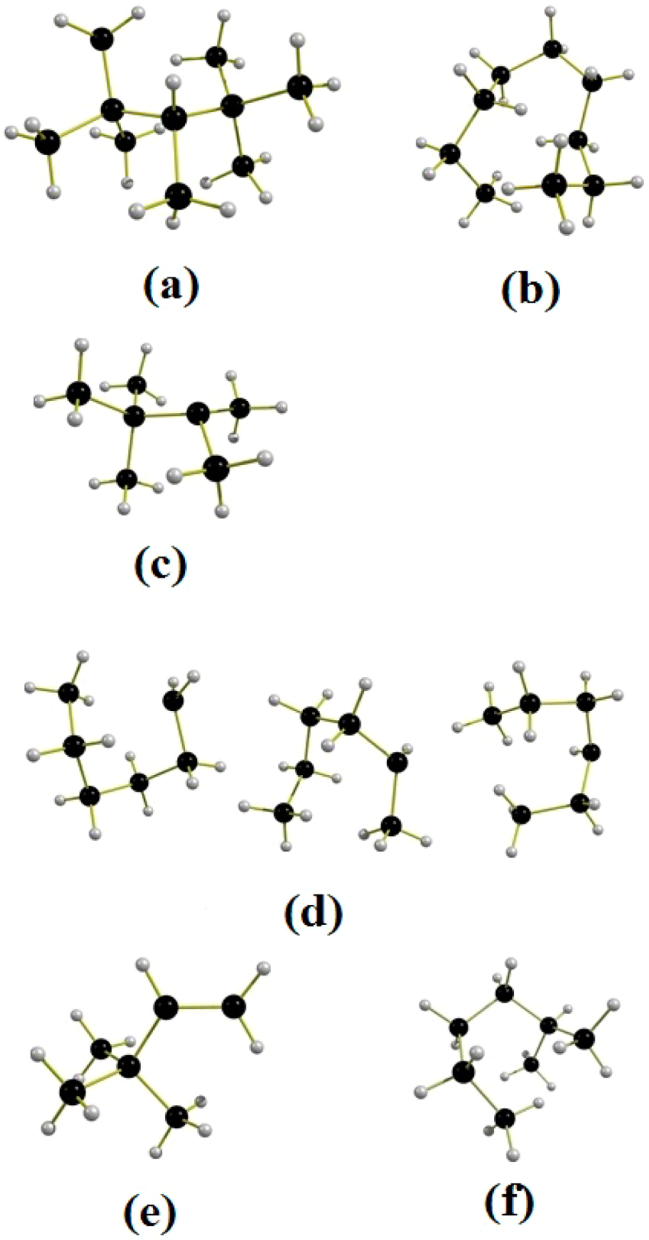

Figure 1. M06-L/MG3S optimized global-minimum-energy structures of the largest representatives for each of the classes of systems considered in the present work: (a) fully branched silanes, $Si_{10}H_{22}$-FB; (b) unbranched silanes, *n*-Si_9H_{20}; (c) fully branched silyl radicals, Si_7H_{15}-FB; (d) unbranched silyl radicals, types I, II, and III, Si_6H_{13}; (e) fully branched silenes, Si_6H_{12}-FB; and (f) *iso*-Si_7H_{16}. Si atoms are black, and H atoms are light gray.

Table 4. Systems Studied in the Present Investigation and the Total Number of Torsions Present in Each System

systems, Si_nH_m	m	torsions
Si_2H_6, Si_3H_8, fully branched, *iso*-Si_7H_{16}, and unbranched silanes	$2n + 2$	$n - 1$
Si_2H_5, Si_3H_7, fully branched and unbranched silyl radicals	$2n + 1$	$n - 1$
Si_3H_6 and fully branched silenes	$2n$	$n - 2$

For the *n*-silanes, as we increase the chain length, the number of torsions increases, and the number of conformational structures increases dramatically with increase in the number of silicon atoms. We denote the number of torsions that generate distinguishable structures as t_D. Note that $t_D \leq t$ because internal rotation of an SiH_3 group does not generate additional distinguishable structures. If all torsions were independent and ideal, then t_D 3-fold torsions would generate $3t_D$ structures. In our case, the t_D values for *n*-Si_5H_{12}, *n*-Si_6H_{14}, *n*-Si_7H_{16}, *n*-Si_8H_{18}, and *n*-Si_9H_{20} are 2, 3, 4, 5, and 6, respectively; therefore, ideal torsions would generate 9, 27, 81, 243, and 729 structures. However, the torsions are strongly coupled, and the numbers of distinguishable structures for these *n*-silanes are respectively 7, 21, 44, 139, and 543 (as given in Table 5). Among these, we found 3, 10, 21, 68, and 270 pairs of optical isomers, respectively, for *n*-Si_5H_{12} through *n*-Si_9H_{20}. For *iso*-Si_7H_{16}, we have 34 distinguishable structures (17 pairs of optical isomers).

Table 5. Number of Distinguishable Structures Obtained for Unbranched Silanes, 2-Silylhexasilane, and Unbranched Silyl Radicals[a]

n	silane, Si_nH_{2n+2}	silyl radical, Si_nH_{2n+1}
4	3	type I, 9; type II, 6
5	7	type I, 27; type II, 18; type III, 11
6	21	type I, 79; type II, 48; type III, 50
7	44	
7-iso[b]	34	
8	139	
9	543	

[a]The results are obtained by optimizing the structures with M06-L/MG3S. [b]7-iso denotes 2-silylhexasilane (also called *iso*-Si_7H_{16}), which is a branched silane, whereas other species in this table are unbranched.

Tables 6 and 7 give the number of structures in each of four relative conformational energy ranges for the *n*-silanes and *iso*-Si_7H_{16} with respect to the global minimum geometry for each species. The MS-T calculations show that up to *n*-heptasilane, the contribution of the lowest-energy distinguishable structures to the partition function is considerable. However, in the cases of *n*-octasilane and *n*-nonasilane, the higher-energy structures dramatically dominate. For example, for *n*-octasilane, the higher-energy structures (defined here as structures more than 2 kcal/mol above the global minimum) contribute 93.6% of the partition function and hence 93.6% of the population at 1000 K, whereas for *n*-nonasilane, the contribution is 98.5% at

dx.doi.org/10.1021/ja410498d | J. Am. Chem. Soc. 2014, 136, 2786−2799

Table 6. Number of Distinguishable Structures in Each Relative Conformational Energy Range for the Unbranched Species with n = 4−6

			unbranched silyl radicals[b]		
n	energy (kcal/mol)	unbranched silanes[a]	I	II	III
4	0.0−0.5	3	3	4	
	0.5−1.0	0	6	2	
	1.0−2.0	0	0	0	
	>2.0	0	0	0	
	total	3	9	6	
5	0.0−0.5	4	4	10	4
	0.5−1.0	3	9	0	2
	1.0−2.0	0	14	8	5
	>2.0	0	0	0	0
	total	7	27	18	11
6	0.0−0.5	10	6	2	2
	0.5−1.0	2	20	4	8
	1.0−2.0	9	37	26	18
	>2.0	0	16	16	22
	total	21	79	48	50

[a]These results are calculated by BMC-CCSD//M06-L/MG3S. [b]These results are calculated by G3SX(MP3)//M06-L/MG3S.

Table 7. Number of Distinguishable Structures in Each Relative Conformational Energy Range for Silanes with n = 7−9 and 2-Silylhexasilane[a]

n	energy (kcal/mol)	number
7[b]	0.0−0.5	12
	0.5−1.0	10
	1.0−2.0	15
	>2.0	7
	total	44
7-iso[c]	0.0−0.5	10
	0.5−1.0	6
	1.0−2.0	14
	>2.0	4
	total	34
8[b]	0.0−0.5	2
	0.5−1.0	18
	1.0−2.0	50
	>2.0	69
	total	139
9[b]	0.0−0.5	4
	0.5−1.0	14
	1.0−2.0	134
	>2.0	391
	total	543

[a]These results are calculated by BMC-CCSD//M06-L/MG3S. [b]Unbranched. [c]7-iso denotes 2-silylhexasilane or *iso*-Si_7H_{16}.

1000 K. At 300 K, the contributions of the higher-energy structures to the populations for octasilane and nonasilane are 69.8% and 82.8%, respectively.

For unbranched Si oligomers up to 8, we found that the all-anti conformer is the least stable. This disagrees with the earlier results of Ortiz and co-workers.[15,16] They found the all-anti conformer to be the most stable geometry when optimized with the Hartree−Fock (HF) method, whereas perturbation theory predicts that the all-gauche and all-anti conformers have nearly the same energy, with the all-gauche conformer being more stable by 0.5 kcal/mol.[18] As an example, in our higher-level calculations for n-octasilane, the all-anti conformer is least stable (out of 139 structures), with a relative conformational energy of 3.22 kcal/mol.

The estimated thermodynamic properties for the fully branched, *iso*-Si_7H_{16}, and unbranched silanes are given in Table 8 at temperatures 298 and 1000 K. A more detailed analysis is provided as Tables S1 and S2 of the SI. The fully branched Si_9H_{20} cluster has one chiral center with the groups, −H, $-SiH_3$, $-SiH(SiH_3)_2$, and $-Si(SiH_3)_3$. Hence, we estimated the thermodynamic quantities for both the S- and R-conformers. The free energies of the S- and R-conformers differ by 1.0 kcal/mol at 1000 K. The thermodynamic properties for unbranched silanes are provided in Table S2 of the SI using BMC-CCSD//M06-L/MG3S method for both the MS-T(U) and MS-T(C) methods.

In Figure 2a, we compare our entropy data for Si_2H_6, Si_3H_8, and fully branched silanes at 298 K to the group additivity (GA) and empirical (BAC) results of Wong et al.[8] Our results for these species with one distinguishable structure differ by 3.0 cal mol^{-1} K^{-1} from the GA results of Wong et al.,[8] (n = 3−7) and by 7.9 and 12.2 cal mol^{-1} K^{-1} for the two highest clusters, Si_9H_{20} and $Si_{10}H_{22}$. When compared with the BAC results of Wong et al., our results differ by 3.5 cal mol^{-1} K^{-1}. We believe that these discrepancies in the values are due to the limitations of the BAC and GA results, as discussed further below.

For the unbranched silanes, when we compared our standard entropy values (102.0 cal mol^{-1} K^{-1} and 118.1 cal mol^{-1} K^{-1}, respectively, for Si_4H_{10} and Si_5H_{12}) at 298 K with the GA results of Wong et al.[8,9] (99.8 cal mol^{-1} K^{-1} and 114.7 cal mol^{-1} K^{-1}, respectively, for Si_4H_{10} and Si_5H_{12}), we found a difference of about 3.4 cal mol^{-1} K^{-1}. This difference increases to 8.1 cal mol^{-1} K^{-1} as one increase the chain length up to 9 Si atoms. Comparing with the BAC results of Wong et al. for unbranched tetra- and pentasilanes, we obtained a difference in the values of 2.5 cal mol^{-1} K^{-1}. These differences are attributed in part to the fact that we included all possible distinguishable structures in our calculations for these unbranched systems.

The multistructural and torsional potential anharmonicity effects are further observed when our standard heat capacity data for single-structure Si_3H_8 and fully branched and unbranched silanes are compared with the GA and BAC results of Wong et al.[8,9] The relevant curves are given in Figure 3. In case of the fully branched silanes, as we go to larger cluster size and higher temperatures, deviations in the heat capacity values between our results and both the GA and BAC results of Wong et al.[8] are observed. For the unbranched silanes, the deviations in the heat capacity values between the results are larger than fully branched silane, which is due to the inclusion of more than one structure in the present work. Although there are no experimental results for the higher unbranched silanes, our results show that one can reproduce experiment for the right reason only if one includes multiple structures.

It is observed in this study that branching affects the thermodynamic properties to a negligible extent for smaller clusters (n = 4−6) and to a considerably greater extent for higher homologues. In case of Si_7H_{16}, the values of the Gibbs free energy, enthalpy, entropy, and heat capacity at 1000 K are

dx.doi.org/10.1021/ja410498d | J. Am. Chem. Soc. 2014, 136, 2786−2799

Table 8. Standard State Thermodynamic Properties for Silanes[a]

system	T (K)	G_T° (kcal/mol)	H_T° (kcal/mol)	S_T° (cal mol^{-1} K^{-1})	$C_p^\circ(T)$ (cal mol^{-1} K^{-1})
Silanes (SS-T Approximation)					
Si_2H_6	298	13.4	34.2	69.5	18.8
	1000	−47.8	53.9	101.7	34.3
Si_3H_8	298	20.9	46.4	85.6	27.3
	1000	−57.0	74.5	131.6	48.5
Fully Branched Silanes (SS-T Approximation)					
Si_4H_{10}-FB	298	28.6	58.9	101.8	35.8
	1000	−66.1	95.4	161.4	62.5
Si_5H_{12}-FB	298	35.9	71.3	118.6	43.9
	1000	−75.8	116.0	191.7	76.5
Si_6H_{14}-FB	298	44.5	83.9	132.0	53.9
	1000	−82.6	137.7	220.4	91.3
Si_7H_{16}-FB	298	54.0	96.5	142.8	64.0
	1000	−86.9	159.6	246.5	106.5
Si_9H_{20}-FB (*S*-conformer)	298	71.2	121.2	167.8	81.8
	1000	−98.5	201.8	300.3	135.8
Si_9H_{20}-FB (*R*-conformer)	298	71.0	121.4	169.0	81.8
	1000	−99.5	201.9	301.4	135.6
$Si_{10}H_{22}$-FB	298	80.8	134.2	179.3	91.2
	1000	−102.9	223.8	326.7	150.7
Branched Silanes (MS-T Approximation)					
iso-Si_7H_{16}	298	52.5	97.3	150.2	65.1
	1000	−93.5	159.9	253.4	105.6
Unbranched Silanes (MS-T Approximation)					
Si_4H_{10}	298	28.6	59.0	102.0	36.3
	1000	−66.5	95.7	162.2	62.7
Si_5H_{12}	298	36.4	71.6	118.1	45.8
	1000	−75.7	117.2	192.8	77.3
Si_6H_{14}	298	44.3	84.4	134.6	56.8
	1000	−85.3	138.8	224.1	91.6
Si_7H_{16}	298	52.6	97.7	151.0	65.4
	1000	−94.0	160.5	254.4	105.9
Si_8H_{18}	298	61.4	111.1	166.8	79.5
	1000	−102.6	183.0	285.7	120.2
Si_9H_{20}	298	70.0	124.3	182.2	91.8
	1000	−111.1	205.2	316.2	134.6

[a]These results are calculated by BMC-CCSD//M06-L/MG3S. FB denotes fully branched.

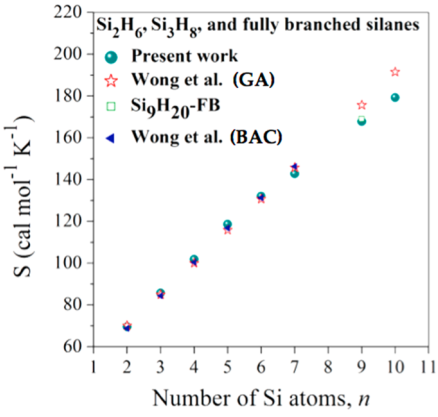

Figure 2. Variations of the standard state entropies at 298 K for single-structure Si_3H_8 and fully branched silanes vs the number of Si atoms, n. The results are calculated by BMC-CCSD//M06-L/MG3S. The group additivity results obtained from the work of Wong et al. (ref 8) and their G3//B3LYP (up to n = 7) results are given for comparison. Since Si_9H_{20} has a chiral center, it has both *S*- and *R*-structures (sinister and rectus). The *S*-conformer is the "Present work".

−86.9 kcal/mol, 159.6 kcal/mol, 246.5 cal mol^{-1} K^{-1}, and 106.5 cal mol^{-1} K^{-1} for fully branched silane, whereas for the unbranched heptasilane, the corresponding values are −94.0 kcal/mol, 160.5 kcal/mol, 254.4 cal mol^{-1} K^{-1}, 105.9 cal mol^{-1} K^{-1}, and for *iso*-Si_7H_{16}, the thermodynamic quantities at 1000 K are −93.5 kcal/mol, 159.9 cal mol^{-1}, 253.4 cal mol^{-1} K^{-1}, and 105.6 cal mol^{-1} K^{-1}, respectively. This clearly indicates that Gibbs free energy and entropy changes considerably (about 8 units) with branching. However, for *iso*-Si_7H_{16} where the branching is only at the terminal Si atom, the values differ only by 0.3−1 unit with respect to its unbranched counterpart.

Silyl Radicals. Silanes may be oxidized when they form radicals; the radicals are formed by the abstraction of H$^\bullet$ from the corresponding silanes. The total number of torsions present in fully branched and unbranched silyl radicals is one less than the number of Si atoms, i.e., n − 1. For the fully branched silyl radicals, we limit our calculations to seven Si atoms, whereas for the unbranched radicals, the calculations were done for n = 4−6. All of the fully branched silyl radicals considered here have only one distinguishable structure, and unbranched systems have multiple distinguishable structures.

dx.doi.org/10.1021/ja410498d | J. Am. Chem. Soc. 2014, 136, 2786−2799

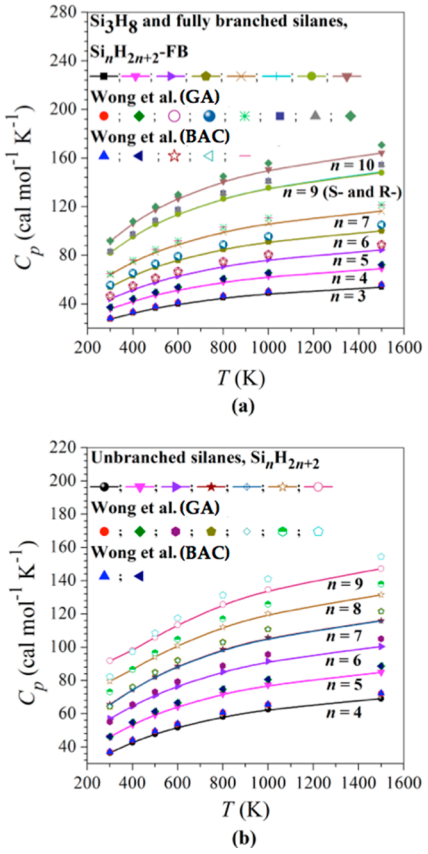

Figure 3. Variation with temperature of the standard state heat capacities for (a) single-structure Si_3H_8 and fully branched silanes, Si_nH_{2n+2}-FB (n = 4−10), and (b) unbranched silanes, Si_nH_{2n+2} (n = 4−9). The results are calculated by BMC-CCSD//M06-L/MG3S. For comparison, the entropy and heat capacity values from the work of Wong et al.[8] are also shown. For the fully branched silanes, the G3//B3LYP results are given from n = 3 to 7, whereas for the unbranched silanes, the results are given for tetra- and pentasilanes.

We distinguish three kinds of unbranched radicals, primary ones, which we label as type I, and two kinds of secondary ones that we label II and III. Si_4H_9 radicals have two radical types: type I and type II. Si_4H_9 contains 4 Si atoms and can form one terminal radical (type I), where the radical position is centered on either of the terminal $-SiH_3$ groups. The radical type II has the active site at a Si adjacent to a terminal $-SiH_3$. For the other two unbranched systems, Si_5H_{11} and Si_6H_{13}, there are three radical types: type I, type II, and type III. Figure 1d depicts the M06-L/MG3S optimized global minimum geometries for the three different radical types of Si_6H_{13}. For the tetrasilyl radicals, we get 9 and 6 distinguishable structures, respectively, for type I and II. In the case of Si_5H_{11} radicals, the number of distinguishable structures is found to be 27, 18, and 11 for types I, II, and III, respectively. For Si_6H_{13} unbranched radicals, the number of distinguishable structures is 79, 48, and 50, respectively, for types I, II, and III. These are presented in Table 5. Of these structures, we found 4 and 3 pairs of optical isomers, respectively, for Si_4H_9 radicals type I and II. For Si_5H_{11} radicals type I, II, and III, the number of pairs of optical isomers is 13, 9, and 5, respectively. In case of Si_6H_{13} radicals of type I, II, and III, we obtained 39, 24, and 25 pairs of optical isomers.

Removal of one H makes a system less symmetric than the corresponding silane, and Table 5 shows that the number of distinguishable structures increases. For the type I radical, this is quite obvious since the number of strongly coupled torsions (t_D) also increases by one. However, for the other two radical types, the "t_D" values are the same as that of silanes—yet we get more distinguishable structures; this illustrates the non-separable nature of the coupled torsions. For pentasilyl radical, the type III radicals have less distinguishable structures compared to type II because the type III radical is more symmetric.

The relative conformational energy ranges for the unbranched silyl radicals are presented in Table 6. As for silanes, the structures have relative conformational energies within 2 kcal/mol for n = 4 and 5 radicals, but for the Si_6H_{13} unbranched radical, there are many structures with relative conformational energy greater than 2 kcal/mol.

The estimated thermodynamic properties are given in Table 9 for Si_2H_5, Si_3H_7, and fully branched silyl radicals and in Table 10 for unbranched silyl radicals. The trends are similar to those for the parent closed-shell species. The entropies at 298.15 K for the single-structure silyl radicals are plotted in Figure 4a, and the heat capacities for radicals with n = 3−7 are plotted for temperatures 300−1000 K in Figure 4b. The corresponding values of the $S_{298.15}$ and C_p from the work of Bhandarkar et al.[4] and Katzer et al.[2] are also plotted for comparison, and they are seen to deviate from our multistructural results at the higher temperatures.

Silenes. The final category of systems that we studied in the present work is silenes. They are the Si analogue of alkenes with

Table 9. Standard Thermodynamic Properties for Single-Structure Silyl Radicals[a]

system	T (K)	G_T° (kcal/mol)	H_T° (kcal/mol)	S_T° (cal mol^{-1} K^{-1})	$C_p^\circ(T)$ (cal mol^{-1} K^{-1})
Si_2H_5	298	7.4	28.2	70.0	17.7
	1000	−53.0	45.8	98.8	30.0
Si_3H_7	298	15.1	40.8	86.3	25.6
	1000	−61.9	66.5	128.5	44.0
Si_4H_9-FB	298	22.6	53.3	103.2	33.1
	1000	−71.4	87.1	158.5	57.9
Si_5H_{11}-FB	298	29.9	65.5	119.2	43.3
	1000	−81.2	108.1	189.3	72.2
Si_6H_{13}-FB	298	38.7	78.4	133.2	52.9
	1000	−88.0	129.8	217.8	86.5
Si_7H_{15}-FB	298	48.2	91.4	145.0	62.2
	1000	−92.7	151.8	244.5	101.4

[a]These results are calculated by G3SX(MP3)//M06-L/MG3S. FB denotes fully branched.

dx.doi.org/10.1021/ja410498d | J. Am. Chem. Soc. 2014, 136, 2786−2799

Table 10. Standard Thermodynamic Properties for Unbranched Silyl Radicals[a]

system	type	T (K)	G_T° (kcal/mol)	H_T° (kcal/mol)	S_T° (cal mol^{-1} K^{-1})	$C_p^\circ(T)$ (cal mol^{-1} K^{-1})
Si_4H_9	I	298	22.0	53.1	104.3	35.0
		1000	−73.4	87.6	161.0	58.4
	II	298	22.4	53.3	103.9	34.7
		1000	−72.6	87.7	160.3	58.2
Si_5H_{11}	I	298	29.8	65.9	121.2	44.3
		1000	−83.2	109.1	192.2	72.8
	II	298	30.1	66.2	120.9	43.7
		1000	−82.4	109.1	191.4	72.5
	III	298	30.6	66.2	119.7	44.7
		1000	−81.4	109.5	190.9	72.7
Si_6H_{13}	I	298	37.9	79.0	137.9	54.2
		1000	−92.5	130.8	223.3	87.1
	II	298	38.8	79.8	137.6	53.3
		1000	−91.0	131.4	222.5	86.9
	III	298	38.8	79.8	137.5	53.9
		1000	−91.2	131.5	222.7	86.9

[a]These results are calculated by G3SX(MP3)//M06-L/MG3S.

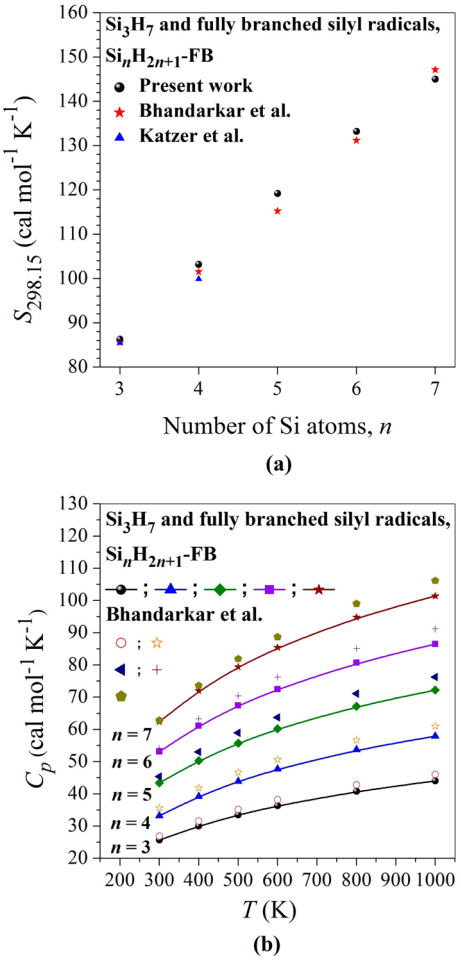

Figure 4. Variation of (a) the standard state entropies (298.15 K and 1 bar pressure) for single-structure Si_3H_7 and fully branched silyl radicals, Si_nH_{2n+1}-FB (n = 4−7), with the number of Si atoms, n, and (b) the standard state heat capacities for single-structure Si_3H_7 and fully branched silyl radicals, Si_nH_{2n+1}-FB (n = 4−7), with temperature. The results are calculated by G3SX(MP3)//M06-L/MG3S. For comparison, the entropy and heat capacity values from the work of Bhandarkar et al. (ref 4) and Katzer et al. (ref 2) are also shown.

the chemical formula Si_nH_{2n} and n − 2 torsions; the number of torsions is one less than in the other systems due to the double bonds. The silenes considered in the present investigation are all fully branched (except Si_3H_6), and have one distinguishable structure. The M06-L/MG3S optimized global minimum geometry for fully branched hexasilene, Si_6H_{12}-FB, is presented in Figure 1e. Table 11 gives the thermodynamic properties for the four silenes studied at temperatures 298 and 1000 K. In Figure 5, we plotted our computed standard entropies for the silenes along with the GA and BAC results of Wong et al.[8] and the empirical results of Katzer et al.[2] at 298.15 K and 1 bar. The two curves show similar trends; however, the group additivity values differ by about 3.6 cal mol^{-1} K^{-1} from the present multistructural values. When compared with the BAC results, the values differ by 1.1 cal mol^{-1} K^{-1}, whereas the difference with the data of Katzer et al. is large (5.5 cal mol^{-1} K^{-1}).

Roles of Multiple Structures and Torsional Potential Anharmonicities. As mentioned earlier, one of the purposes of the present study is to demonstrate and quantify the role of multiple structures and torsional potential anharmonicities in determining the thermodynamic properties for silicon hydrides and their radicals. Figures 6−8 illustrate the effect of torsional potential anharmonicity and multiple structures in these systems. The partition function ratio $Q_{MS\text{-}T}/Q_{MS\text{-}QH}$ shows the effect of torsional potential anharmonicities, whereas the ratio $Q_{MS\text{-}QH}/Q_{SS\text{-}QH}$ depicts the role of multiple structures where the single-structure result corresponds to the global minimum geometry for a given system. In Figure 6, the torsional anharmonicity ratio, i.e., $Q_{MS\text{-}T}/Q_{MS\text{-}QH}$, is plotted at various temperatures. As the chain length of the unbranched silanes increases, the number of torsions also increases, and this might naïvely be expected to increase the MS-T partition functions, thereby increasing the partition function ratio. However, this is not the case, and instead, we found a decreasing $Q_{MS\text{-}T}/Q_{MS\text{-}QH}$ ratio with increase in chain length. This is because torsional potential anharmonicity becomes more important. A considerable difference in the ratio is also observed at lower temperatures for the two heptasilane isomers, the *n*-form and the *iso*-form. Figure 7 plots the ratio $Q_{MS\text{-}QH}/Q_{SS\text{-}QH}$ with temperature. Since the ratio is very large for Si_9H_{20} in comparison with the other silanes, we provide the ratios for n = 4−8 clusters in the inset of Figure 7. (More detailed

dx.doi.org/10.1021/ja410498d | J. Am. Chem. Soc. 2014, 136, 2786−2799

Table 11. Standard Thermodynamic Properties for Single-Structure Silenes[a]

system	T (K)	G_T° (kcal/mol)	H_T° (kcal/mol)	S_T° (cal mol^{-1} K^{-1})	$C_p^\circ(T)$ (cal mol^{-1} K^{-1})
Si_3H_6	298	11.2	35.6	81.8	25.3
	1000	−61.9	59.8	121.7	40.5
Si_4H_8-FB	298	18.3	48.4	101.0	33.2
	1000	−73.5	80.7	154.3	54.4
Si_5H_{10}-FB	298	27.8	61.0	111.4	41.2
	1000	−76.5	101.5	178.1	68.4
Si_6H_{12}-FB	298	35.0	73.0	127.7	52.1
	1000	−87.0	122.9	209.9	83.1

[a]These results are calculated by G3SX(MP3)//M06-L/MG3S. FB denotes fully branched.

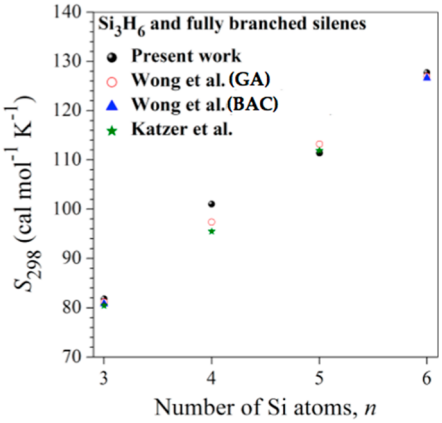

Figure 5. Variations with the number, n, of Si atoms of the standard state entropies at 298 K and 1 bar pressure for single-structure Si_3H_6 and fully branched silenes. The results are calculated by G3SX-(MP3)//M06-L/MG3S. The group additivity results from the work of Wong et al. (ref 8) and Katzer et al. (ref 2) are given for comparison.

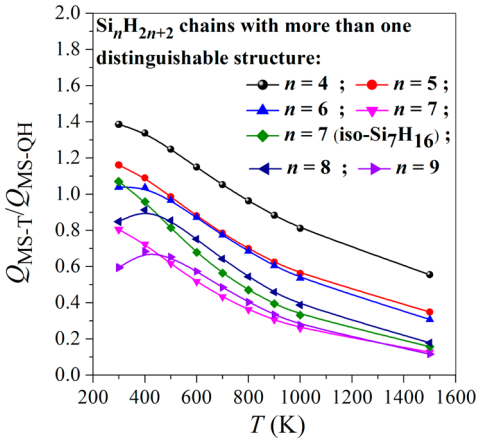

Figure 6. Variations with temperature of the partition function ratios, Q_{MS-T}/Q_{MS-QH}, for unbranched silanes. The curves represent the effect of torsional potential anharmonicity. The results are calculated by BMC-CCSD//M06-L/MG3S.

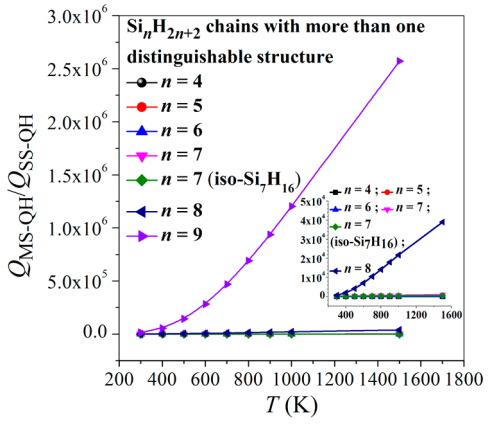

Figure 7. Variations with temperature of the partition function ratios, Q_{MS-QH}/Q_{SS-QH}, for unbranched silanes. The curves represent the effect of the presence of multiple structures. The results are calculated by BMC-CCSD/MG3S//M06-L/MG3S.

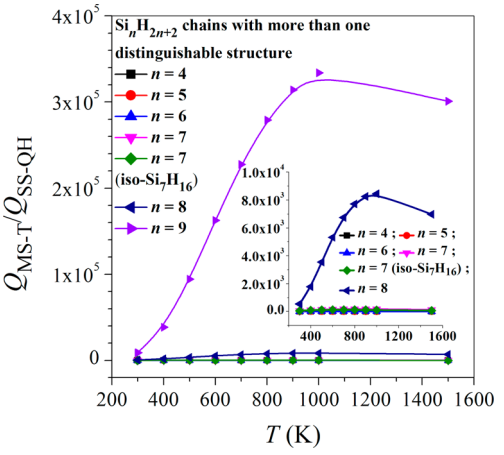

Figure 8. Variations with temperature of the partition function ratios, Q_{MS-T}/Q_{SS-QH}, for unbranched silanes. The curves represent the combined effects of the presence of multiple structure and torsional potential anharmonicity. The results are calculated by BMC-CCSD//M06-L/MG3S.

information about the partition function ratios is provided in Tables S8 and S9 of the SI.) Figure 7 clearly demonstrates the large effect of multiple structures on the partition functions and thermodynamic properties in these systems. The values of the ratio for Si_8H_{18} (139 structures) and Si_9H_{20} (543 structures) are 2.2×10^4 and 1.2×10^6, respectively, at 1000 K, whereas the ratios for the lower silanes are of the order of 10^1 and 10^2. The combined effect of multiple structures and torsional anharmonicities is given in Figure 8, where we plot the MS-T partition function ratio, Q_{MS-T}/Q_{SS-QH}, as a function of temperature. The curves follow the same trend as that of Figure 7 up to 1000 K since the contribution of multiple structures is large compared to torsional potential anharmonicities. However, after 1000 K, the curves follow a decreasing trend with temperature irrespective of the chain length. This is due to the fact that torsional potential anharmonicity ratio reduces considerably at high temperatures.

dx.doi.org/10.1021/ja410498d | J. Am. Chem. Soc. 2014, 136, 2786−2799

Table 12. Difference in the Standard-State Gibbs Free Energy, Enthalpy, and Entropy between the MS-T and SS-QH Approximations for Species with More Than One Distinguishable Structure

species	T (K)	$(G_T^\circ - H_0^\circ)^{\text{MS-T}} - (G_T^\circ - H_0^\circ)^{\text{SS-QH}}$ (kcal/mol)	$(H_T^\circ - H_0^\circ)^{\text{MS-T}} - (H_T^\circ - H_0^\circ)^{\text{SS-QH}}$ (kcal/mol)	$(S_T^\circ)^{\text{MS-T}} - (S_T^\circ)^{\text{SS-QH}}$ (cal mol^{-1} K^{-1})
		Branched Silanes (BMC-CCSD//M06-L/MG3S)		
iso-Si_7H_{16}	298	−2.4	1.2	12.0
	1000	−9.3	−1.6	7.7
		Unbranched Silanes (BMC-CCSD//M06-L/MG3S)		
Si_4H_{10}	298	−1.2	0.1	4.3
	1000	−3.2	−1.6	1.7
Si_5H_{12}	298	−1.3	0.4	5.8
	1000	−4.2	−1.4	2.7
Si_6H_{14}	298	−1.2	0.9	7.1
	1000	−5.1	−1.2	3.9
Si_7H_{16}	298	−2.3	1.8	13.3
	1000	−10.2	−0.9	9.1
Si_8H_{18}	298	−4.1	2.7	22.8
	1000	−19.3	0.1	19.5
Si_9H_{20}	298	−5.8	3.2	30.2
	1000	−26.7	0.8	27.4
		Unbranched Silyl Radicals (G3SX(MP3)//M06-L/MG3S)		
Si_4H_9, type I	298	−0.8	0.1	3.0
	1000	−1.7	−1.7	0.1
Si_4H_9, type II	298	−0.8	0.0	2.8
	1000	−1.6	−1.7	−0.1
Si_5H_{11}, type I	298	−2.1	0.6	9.0
	1000	−7.1	−1.6	5.5
Si_5H_{11}, type II	298	−1.7	0.5	7.3
	1000	−5.5	−1.7	3.7
Si_5H_{11}, type III	298	−1.3	0.5	6.4
	1000	−4.8	−1.3	3.5
Si_6H_{13}, type I	298	−2.7	1.3	13.3
	1000	−10.6	−1.3	9.3
Si_6H_{13}, type II	298	−2.9	1.7	15.5
	1000	−12.1	−0.8	11.4
Si_6H_{13}, type III	298	−2.8	1.7	14.8
	1000	−11.8	−0.7	11.1

Entropic Effects on the Thermochemistry. In order to further quantify the effects of multiple structures, torsional potential anharmonicity, and in particular, the entropic effects, we have also determined the following quantities, $(G_T^\circ - H_0^\circ)^{\text{MS-T}} - (G_T^\circ - H_0^\circ)^{\text{SS-QH}}$, $(H_T^\circ - H_0^\circ)^{\text{MS-T}} - (H_T^\circ - H_0^\circ)^{\text{SS-QH}}$, and $(S_T^\circ)^{\text{MS-T}} - (S_T^\circ)^{\text{SS-QH}}$ at temperatures 298 and 1000 K for all the unbranched species and *iso*-Si_7H_{16}. The values are given in Table 12. The SS-QH thermodynamic quantities are calculated using the M06-L/MG3S optimized geometry of the global minimum structure (the global minimum is assigned a relative conformational energy of 0) and Hessian. When the global minimum structure has a mirror image, then we use weight =1 in the MS-QH calculations. It has been observed that for the unbranched silanes and silyl radicals, the Gibbs free energy increases in magnitude at higher temperature and for larger cluster size in the MS-T approximation relative to the SS-QH approximation. If we write $G = H - TS$, then we find that the difference in $|TS|$ is larger than the difference in $|H|$. For example, in the case of Si_8H_{18} at 298 K, the enthalpy difference is 2.7 kcal/mol, but the Gibbs free energy difference is −4.1 kcal/mol. The entropy difference is found to be 22.8 cal mol^{-1} K^{-1}. For the type I Si_6H_{13} silyl radical, although the enthalpy difference is 1.3 kcal/mol at 298 K, the difference in the Gibbs free energy is −2.7 kcal/mol. This is solely due to the huge entropy difference (13.3 cal mol^{-1} K^{-1}) that arises because of the presence of more than one structure. We found an entropy difference of 30.2 and 27.4 cal mol^{-1} K^{-1} at 298 and 1000 K, respectively, for the highest unbranched silane, Si_9H_{20}. Table 12 clearly shows that multistructural effects dominate the entropy. This high entropy difference plays an important role in influencing the Gibbs free energies values, which is related to the equilibrium constant of a reaction. For plasma chemistry, the process of nucleation, i.e., aggregation of smaller clusters to form larger ones, is one of the most crucial processes and a good estimation of the nucleation rate is therefore essential.

Group Additivity (GA) Methods and Their Limitations. In this section, we discuss the group additivity results obtained in previous studies for silicon hydrides and their limitations. Although GA methods have been applied to many systems in order to calculate physicochemical properties, they do have well-known limitations. The errors in group additivity schemes are of two kinds: (1) the error in the experimental data and/or quantum chemical calculations on which the GA parametrization is based and (2) the error inherent in assuming that a group additivity scheme holds. Errors of second kind include not only nonlocal electronic structure effects (converged CI is not group additive), but also nonlocal vibrational effects (the exact vibrational energy of an

dx.doi.org/10.1021/ja410498d | J. Am. Chem. Soc. 2014, 136, 2786−2799

anharmonic molecular system at either 0 K or finite temperature is not group additive) and also multiple structure effects (the difference between the single-structure results and the correct multiple structure results is not group additive because the number and type of multiple structures depends on some nonlocal aspects of the molecular system).

Swihart and Girshick[3] developed a group additivity method to estimate the thermodynamic quantities for arbitrary silanes, silenes, and silylenes in the temperature range 300−1500 K. Their method is based on the thermochemical results obtained by Katzer et al.,[2] where standard state enthalpies and entropies for 143 silicon hydride compounds were estimated using empirically corrected wave function calcuations. The group additivity method of Swihart and Girshick[3] follows the same technique that was used by Benson for the prediction of thermochemical properties of hydrocarbons.[58] The group contribution values were determined by a linear least-squares fit to the properties of 71 silicon hydride species studied by Katzer et al.[2] A limitation of this method is that the resulting group additivity values are not exhaustive and can be applied only to molecules with a single functionality, e.g., a double bond or a silylene center. In order to alleviate this problem, Wong et al.[8] developed an empirical bond additivity correction (BAC) and fitted the group additivity scheme to the corrected values. Their BAC results for 131 small-to-medium silicon−hydrogen molecules were used to develop group additivity values that can be applied to molecules with multiple functionalities.

These group additivity methods are based on single structures. Katzer et al.[2] calculated thermodynamic properties for neutral silicon hydride molecules and radicals with up to five Si atoms. Whereas we find seven structures for Si_5H_{12} and 11 for Si_5H_{11}, they employed only one structure for each molecule and radical studied. We find (as shown in Table 12) that the single-structure approximation causes errors in free energy of up to 4.2 kcal/mol for Si_5H_{12} and up to 7.1 kcal/mol or Si_5H_{11}, with the dominant contributions (2.7 and 5.5 kcal/mol, respectively) coming from the entropy. Katzer made empirical corrections to their calculated enthalpies based on ΔH_{298} for species with up to three Si atoms, but since the multistructural effects in chain molecules increase rapidly with both the number of Si atoms and the temperature, and since they made no corrections to the entropy, their results cannot be expected to be reliable. The group additivity parameters of Swihart and Girshick[3] are fitted to the results of Katzer et al.[2] as mentioned earlier, and so they suffer from the same problem. Wong et al.,[8] although carrying out thermochemical calculations for linear tetra- and pentasilanes, still neglect the presence of more than one distinguishable structure in those systems while calculating the group additivity values. Hence, the thermochemical properties obtained by the previous group additivity approaches are all questionable.

For fully branched Si_5H_{12}, we found differences of 2.4 cal mol^{-1} K^{-1} in S_{298} and 2.4−4 cal mol^{-1} K^{-1} in the heat capacity at 300−1500 K from the results of Wong et al.,[8] whose values are based on only a single structure. Consider also the case of *iso*-Si_7H_{16}. The M06-L/MG3S optimized global minimum geometry for this system is presented in Figure 1f. The group additivity methods are based on considering each isomer of Si_7H_{16} to have only one structure, which is not the case; we found a difference of about 6.6 cal mol^{-1} K^{-1} in the entropy value of *iso*-Si_7H_{16} at 298 K when compared with the work of Wong et al.[8] and a similarly large difference of 5.6 cal mol^{-1} K^{-1} for unbranched Si_7H_{16}.

Cost Effectiveness. Computational cost is one of the key issues in the present study, and it depends on the system size. For optimizing and performing vibrational frequency calculations of the simplest silane, Si_2H_6, it took 342.18 s per processor when performed on a single node (8 processors) of ITASCA. For performing the same calculations on the highest fully branched silane, $Si_{10}H_{22}$-FB, it took 69250 s per processor. For the unbranched silanes, the timing for the optimization and vibrational frequency calculations depend on the initial geometry for a particular silane. The *MSTor* calculations, however, completes within 10−15 s for the highest silanes, $Si_{10}H_{22}$-FB and Si_9H_{20}.

Zero of Energy. In the tables, $G_T°$ and $H_T°$ are given for the zero of energy set equal to the potential energy of the global minimum, and they can be converted to the standard thermodynamic quantities $G_T° - H_0°$ and $H_T° - H_0°$ by subtracting the zero point energy (ZPE); for this purpose, the ZPE values of all calculated species are given in the SI.

CONCLUSIONS

We applied the recently developed multistructural torsion approximation with a coupled potential to calculate the partition functions, enthalpies, heat capacities, entropies, and free energies for unbranched silanes, fully branched silanes, *iso*-Si_7H_{16}, unbranched and fully branched silyl radicals, and silenes in the temperature range of 298−1500 K. Our results for the thermodynamic properties of the silicon−hydrogen containing compounds differ considerably from previous results, based on group additivity and other empirical aspects, and this is due in part to the group additivity methods being based on a single structure for each stoichiometry and hence being devoid of any multistructural effects. The present investigation demonstrates the quantitative importance of multiple structures and torsional anharmonicity in these systems and—by extension—in chain molecules more generally. The present study shows that electronic structure calculations, when combined with multistructural statistical thermodynamic methods, can now be used for calculating realistic thermodynamic properties needed for plasma nucleation modeling, and that the resulting thermodynamic properties show large conformational entropies. We can confidently use the present approach to predict the thermodynamic quantities even for molecules with multiple torsions and for temperatures where there are no available experimental or empirical data.

Most textbooks factor molecular partition functions into three factors: electronic, harmonic or quasiharmonic vibrational, and rotational. This commonly used approximation neglects the conformational contribution, which may be very large, especially for chain molecules like unbranched silanes. The present research quantifies this contribution and shows that it can lead to large effects on entropies, decreasing the free energy by as much as 28.4 kcal/mol for the systems in this work. We hope that the new thermodynamic values obtained here will allow more realistic modeling of nanodusty plasmas and that the warning about the incorrect conclusions that can be drawn when conformational entropy is neglected will be heeded more broadly.

■ ASSOCIATED CONTENT

Supporting Information

M06-L/MG3S optimized Cartesian coordinates for the global minimum geometries for each system studied in the present investigation; the absolute energies in hartrees for all of the systems whose geometries were optimized; thermodynamic quantities in the temperature range 298−1500 K, as calculated by the M06-L/MG3S, BMC-CCSD//M06-L/MG3S, and G3SX(MP3)//M06-L/MG3S methods by using both the MS-T(C) and MS-T(U) approximations; the partition function ratios for the unbranched silanes in both the MS-T(C) and MS-T(U) approximations; comparison of the entropies and heat capacities between our results, the group additivity results and empirical results of Wong et al., and empirical results of Katzer et al.; additional computational details; comparison of calculations with coupled and uncoupled potentials; and zero-point energies of all molecules studied. This material is available free of charge via the Internet at http://pubs.acs.org.

■ AUTHOR INFORMATION

Corresponding Author

truhlar@umn.edu

Notes

The authors declare no competing financial interest.

■ ACKNOWLEDGMENTS

The authors thank Steven L. Girshick, Mark J. Kushner, Rubén Meana-Pañeda, Mark T. Swihart, and Jingjing Zheng for valuable suggestions and assistance. This work is supported by the National Science Foundation under Award No. CHE11-24752.

■ REFERENCES

(1) Bhandarkar, U. V.; Kortshagen, U. R.; Girshick, S. L. *J. Phys. D.: Appl. Phys.* **2003**, *36*, 1399.
(2) Katzer, G.; Ernst, M. C.; Sax, A. F.; Kalcher, J. *J. Phys. Chem. A* **1997**, *101*, 3942.
(3) Swihart, M. T.; Girshick, S. L. *J. Phys. Chem. B* **1999**, *103*, 64.
(4) Bhandarkar, U. V.; Swihart, M. T.; Girshick, S. L.; Kortshagen, U. R. *J. Phys. D.: Appl. Phys.* **2000**, *33*, 2731.
(5) Li, C. P.; Li, X. J.; Yang, J. C. *J. Phys. Chem. A* **2006**, *110*, 12026.
(6) Xu, W. G.; Yang, J. C.; Xiao, W. S. *J. Phys. Chem. A* **2004**, *108*, 11345.
(7) Swihart, M. T. *J. Phys. Chem. A* **2000**, *104*, 6083.
(8) (a) Wong, H.; Alva Nieto, J. C.; Swihart, M. T.; Broadbelt, L. J. *J. Phys. Chem. A* **2004**, *108*, 874. (b) Wong, H.; Li, X.; Swihart, M. T.; Broadbelt, L. J. *J. Phys. Chem. A* **2004**, *108*, 10122.
(9) Ho, P.; Coltrin, M. E.; Binkley, J. S.; Melius, C. F. *J. Phys. Chem.* **1986**, *90*, 3399.
(10) Oyedepo, G. A.; Peterson, C.; Wilson, A. K. *J. Chem. Phys.* **2011**, *135*, 094103.
(11) Chang, Y.; Li, G.; Gao, A.; Chen, H.; Li, Q.-s. *Theor. Chem. Acc.* **2011**, *130*, 1009.
(12) Yang, J. C.; Bai, X.; Li, C. P.; Xu, W. G. *J. Phys. Chem. A* **2005**, *109*, 5717.
(13) Adamczyk, A.; Broadbelt, L. J. *J. Phys. Chem. A* **2011**, *115*, 8969.
(14) Jansik, B.; Schimmelpfennig, B.; Norman, P.; Mochizuki, Y.; Luo, Y.; Ågren, H. *J. Phys. Chem. A* **2002**, *106*, 395.
(15) (a) Ortiz, J. V.; Mintmire, J. W. *J. Am. Chem. Soc.* **1988**, *110*, 4522. (b) Oritz, J. V.; Rohlfing, C. M. *Macromolecules* **1993**, *26*, 7282.
(16) (a) Ho, P.; Coltrin, M. E.; Breiland, W. G. *J. Phys. Chem.* **1994**, *98*, 10138−10147. (b) Apeloig, Y.; Danovich, D. *Organometalics* **1996**, *15*, 350.
(17) (a) Gallagher, A. *Phys. Rev. E* **2000**, *62*, 2690. (b) Seki, S.; Okamoto, K.; Matsui, Y.; Tagawa, S.; Tsuji, H.; Toshimitsu, A.; Tamao, K. *Chem. Phys. Lett.* **2003**, *380*, 141.
(18) Bouchoule, A.; Boufendi, L. *Plasma Sources Sci. Technol.* **1993**, *2*, 204.
(19) (a) Kawabata, H.; Ohmori, S.; Matsushige, K.; Tachikawa, H. *J. Organomet. Chem.* **2006**, *691*, 5525−5530. (b) Islam, S. M.; Hollett, J. W.; Poirier, R. A. *J. Phys. Chem. A* **2007**, *111*, 526.
(20) (a) Inoue, S.; Ichinohe, M.; Sekiguchi, A. *J. Am. Chem. Soc.* **2007**, *129*, 6096. (b) Gordon, M. S.; Francisco, J. S.; Schlegel, H. B. *Adv. Silicon Chem.* **1993**, *2*, 137. (c) Boatz, J. A.; Gordon, M. S.; Hilderbrandt, R. L. *J. Am. Chem. Soc.* **1988**, *110*, 352. (d) Baldridge, K. K.; Boatz, J. A.; Koseki, S.; Gordon, M. S. *Annu. Rev. Phys. Chem.* **1987**, *38*, 211.
(21) Giunta, C. J.; McCurdy, R. J.; Chapple-Sokol, J. D.; Gordon, R. G. *J. Appl. Phys.* **1990**, *67*, 1062.
(22) Frenklach, M.; Ting, L.; Wang, H.; Rabinowitz, M. J. *Isr. J. Chem* **1996**, *36*, 293.
(23) Tonokura, K.; Murasaki, T.; Koshi, M. *J. Phys. Chem. B* **2002**, *106*, 555.
(24) Perrin, J.; Leroy, O.; Bordage, M. *Contrib. Plasma Phys.* **1996**, *36*, 3.
(25) Lynch, B. J.; Truhlar, D. G. *ACS Symp. Ser.* **2007**, *958*, 153.
(26) Zhao, Y.; Truhlar, D. G. *Chem. Phys. Lett.* **2011**, *502*, 1.
(27) Zheng, J.; Yu, T.; Papajak, E.; Alecu, I. M.; Mielke, S. L.; Truhlar, D. G. *Phys. Chem. Chem. Phys.* **2011**, *13*, 10885.
(28) Zheng, J.; Truhlar, D. G. *J. Chem. Theory Comput.* **2013**, *9*, 1356.
(29) Yu, T.; Zheng, J.; Truhlar, D. G. *Chem. Sci.* **2011**, *2*, 2199.
(30) Zheng, J.; Yu, T.; Truhlar, D. G. *Phys. Chem. Chem. Phys.* **2011**, *13*, 19318.
(31) Seal, P.; Papajak, E.; Yu, T.; Truhlar, D. G. *J. Chem. Phys.* **2012**, *136*, 034306.
(32) Seal, P.; Papajak, E.; Truhlar, D. G. *J. Phys. Chem. Lett.* **2012**, *3*, 264.
(33) Papajak, E.; Seal, P.; Xu, X.; Truhlar, D. G. *J. Chem. Phys.* **2012**, *137*, 104314.
(34) Zheng, J.; Seal, P.; Truhlar, D. G. *Chem. Sci.* **2012**, *4*, 200−212.
(35) Seal, P.; Oyedepo, G.; Truhlar, D. G. *J. Phys. Chem. A* **2013**, *117*, 275.
(36) Miller, T. F., III; Clary, D. C. *Phys. Chem. Chem. Phys.* **2004**, *6*, 2563.
(37) Miller, T. F., III; Clary, D. C. *Mol. Phys.* **2005**, *103*, 1573.
(38) Vansteenkiste, P.; Van Speybroeck, V.; Pauwels, E.; Waroquier, M. *Chem. Phys.* **2005**, *314*, 109.
(39) Van Cauter, K.; Van Speybroeck, V.; Vansteeenkiste, P.; Reyniers, M.-F.; Waroquier, M. *ChemPhysChem* **2006**, *7*, 131.
(40) Zheng, J.; Truhlar, D. G. *J. Chem. Theory Comput.* **2013**, *9*, 2875.
(41) Alecu, I. M.; Zheng, J.; Zhao, Y.; Truhlar, D. G. *J. Chem. Theory Comput.* **2010**, *6*, 2872.
(42) Zhao, Y.; Truhlar, D. G. *J. Chem. Phys.* **2006**, *125*, 194101.
(43) (a) McLean, A. D.; Chandler, G. S. *J. Chem. Phys.* **1980**, *72*, 5639. (b) Clark, T.; Chandrasekhar, J.; Spitznagel, G. W.; Schleyer, P. v. R. *J. Comput. Chem.* **1983**, *4*, 294. (c) Frisch, M. J.; Pople, J. A.; Binkley, J. S. *J. Chem. Phys.* **1984**, *80*, 3265. (d) Curtiss, L. A.; Raghavachari, K.; Redfern, C.; Rassolov, V.; Pople, J. A. *J. Chem. Phys.* **1998**, *109*, 7764. (e) Fast, P. L.; Sanchez, M. L.; Truhlar, D. G. *Chem. Phys. Lett.* **1999**, *306*, 407.
(44) Lynch, B. J.; Zhao, Y.; Truhlar, D. G. *J. Phys. Chem. A* **2003**, *107*, 1384.
(45) Frisch, M. J.; Trucks, G. W.; Schlegel, H. B.; Scuseria, G. E.; Robb, M. A.; Cheeseman, J. R.; Scalmani, G.; Barone, V.; Mennucci, B.; Petersson, G. A.; Nakatsuji, H.; Caricato, M.; Li, X.; Hratchian, H. P.; Izmaylov, A. F.; Bloino, J.; Zheng, G.; Sonnenberg, J. L.; Hada, M.; Ehara, M.; Toyota, K.; Fukuda, R.; Hasegawa, J.; Ishida, M.; Nakajima, T.; Honda, Y.; Kitao, O.; Nakai, H.; Vreven, T.; Montgomery, J. A., Jr.; Peralta, J. E.; Ogliaro, F.; Bearpark, M.; Heyd, J. J.; Brothers, E.; Kudin, K. N.; Staroverov, V. N.; Kobayashi, R.; Normand, J.; Raghavachari, K.; Rendell, A.; Burant, J. C.; Iyengar, S. S.; Tomasi, J.; Cossi, M.; Rega, N.; Millam, N. J.; Klene, M.; Knox, J. E.; Cross, J. B.; Bakken, V.;

Adamo, C.; Jaramillo, J.; Gomperts, R.; Stratmann, R. E.; Yazyev, O.; Austin, A. J.; Cammi, R.; Pomelli, C.; Ochterski, J. W.; Martin, R. L.; Morokuma, K.; Zakrzewski, V. G.; Voth, G. A.; Salvador, P.; Dannenberg, J. J.; Dapprich, S.; Daniels, A. D.; Farkas, Ö.; Foresman, J. B.; Ortiz, J. V.; Cioslowski, J.; Fox, D. J. *Gaussian 09*, revision A.1; Gaussian, Inc.: Wallingford, CT, 2009.
(46) Zheng, J.; Mielke, S. L.; Clarkson, K. L.; Truhlar, D. G. *Comput. Phys. Commun.* **2012**, *183*, 1803.
(47) (a) Zheng, J.; Mielke, S. L.; Clarkson, K. L.; Meana-Paneda, R.; Truhlar, D. G. *MSTor*, version 2013; University of Minnesota: Minneapolis, 2013. (b) Zheng, J.; Meana-Pañeda, R.; Truhlar, D. G. *Comput. Phys. Commun.* **2013**, *184*, 2032.
(48) Ruščić, B.; Berkowitz, J. *J. Chem. Phys.* **1991**, *95*, 2416.
(49) Gunn, S. R.; Green, L. G. *J. Phys. Chem.* **1961**, *65*, 779.
(50) Goumri, A.; W-Yuan, J.; Ding, L.; Marshall, P. *Chem. Phys. Lett.* **1993**, *204*, 296.
(51) Chase, M. W., Jr.; Davies, C. A.; Downey, J. R., Jr.; Frurip, D. J.; McDonald, R. A.; Syverud, A. N. *J. Phys. Chem. Ref. Data Suppl.* **1985**, *14*, Suppl. 2.
(52) Zhao, Y.; Lynch, B. J.; Truhlar, D. G. *Phys. Chem. Chem. Phys.* **2005**, *7*, 43.
(53) Zhao, Y.; Lynch, B. J.; Truhlar, D. G. *J. Phys. Chem. A* **2004**, *108*, 4786.
(54) Lynch, B. J.; Truhlar, D. G. *J. Phys. Chem. A* **2003**, *107*, 3898.
(55) Lynch, B. J.; Zhao, Y.; Truhlar, D. G. *J. Phys. Chem. A* **2005**, *109*, 1643.
(56) Curtiss, L. A.; Redfern, P. C.; Raghavachari, K.; Pople, J. A. *J. Chem. Phys.* **2001**, *114*, 108.
(57) Gunn, S. R.; Green, L. G. *J. Phys. Chem.* **1964**, *68*, 946.
(58) Benson, S. *Thermochemical Kinetics*, 2nd ed.; Wiley: New York, 1976.